Summer July 16, 2015

Unimolecular decomposition of formic and acetic acids: A shock tube/laser absorption study

A. Elwardany, *KAUST*
E. F. Nasir, *KAUST*
Et. Es-sebbar, *KAUST*
A. Farooq, *KAUST*

Unimolecular decomposition of formic and acetic acids: A shock tube/laser absorption study

A. Elwardany, E.F. Nasir, Et. Es-sebbar, A. Farooq *

Clean Combustion Research Centre, Division of Physical Sciences and Engineering, King Abdullah University of Science and Technology (KAUST), Thuwal 23955-6900, Saudi Arabia

Available online 16 July 2014

Abstract

The thermal decomposition of formic acid (HCOOH) and acetic acid (CH_3COOH), two carboxylic acids which play an important role in oxygenate combustion chemistry, were investigated behind reflected shock waves using laser absorption. The rate constants of the primary decomposition pathways of these acids:

$HCOOH \rightarrow CO + H_2O$ (R1)
$HCOOH \rightarrow CO_2 + H_2$ (R2)
$CH_3COOH \rightarrow CH_4 + CO_2$ (R3)
$CH_3COOH \rightarrow CH_2CO + H_2O$ (R4)

were measured using simultaneous infrared laser absorption of CO, CO_2 and H_2O at wavelengths of 4.56, 4.18 and 2.93 microns, respectively. Reaction test conditions covered temperatures from 1230 to 1821 K and pressures from 1.0 to 6.5 atm for dilute mixtures of acids (0.25–0.6%) in argon. The rate constants of dehydration (R1) and decarboxylation (R2) reactions of formic acid were calculated by fitting exponential functions to the measured CO, CO_2 and H_2O time-history profiles. These two decomposition channels were found to be in the fall-off region and have a branching ratio, k_1/k_2, of approximately 20 over the range of pressures studied here. The best-fit Arrhenius expressions of the first-order rates of R1 and R2 were found to be:

$k_1(1 \text{ atm}) = 1.03 \times 10^{11} \exp(-25651/T) \text{ s}^{-1} (\pm 37\%)$
$k_1(6.5 \text{ atm}) = 9.12 \times 10^{12} \exp(-30275/T) \text{ s}^{-1} (\pm 32\%)$
$k_2(1 \text{ atm}) = 1.79 \times 10^8 \exp(-21133/T) \text{ s}^{-1} (\pm 41\%)$
$k_2(6.5 \text{ atm}) = 2.73 \times 10^8 \exp(-20074/T) \text{ s}^{-1} (\pm 37\%)$

The rate constants for acetic acid decomposition were obtained by fitting simulated profiles, using an acetic acid pyrolysis mechanism, to the measured species time-histories. The branching ratio, k_4/k_3, was

---

* Corresponding author.
E-mail address: aamir.farooq@kaust.edu.sa (A. Farooq).

found to be approximately 2. The decarboxylation and dehydration reactions of acetic acid appear to be in the falloff region over the tested pressure range:

$$k_3(1 \text{ atm}) = 3.18 \times 10^{11} \ \exp(-28679/T) \ \text{s}^{-1}(\pm 30\%)$$
$$k_3(6 \text{ atm}) = 3.51 \times 10^{12} \ \exp(-31330/T) \ \text{s}^{-1}(\pm 26\%)$$
$$k_4(1 \text{ atm}) = 7.9 \times 10^{11} \ \exp(-29056/T) \ \text{s}^{-1}(\pm 34\%)$$
$$k_4(6 \text{ atm}) = 6.34 \times 10^{12} \ \exp(-31330/T) \ \text{s}^{-1}(\pm 31\%).$$

1. Introduction

Carboxylic acids are compounds which contain one or more carboxyl groups (COOH). They are readily formed during the pyrolysis and oxidation of large oxygenated species. This is particularly important in the modelling of ester-based bio-diesel fuels as carboxylic acids and ketenes are the main products of the pyrolysis of esters [1]. Formic acid (HCOOH) has been shown to be the main product of ethyl formate pyrolysis [2] and acetic acid (CH_3COOH) was observed to be a primary product of ethyl acetate decomposition [2,3]. Formic acid is also an important intermediate during the oxidation of dimethyl ether at low and intermediate temperatures [1] and acetic acid is the major product of acetic anhydride pyrolysis [4,5]. Accurate rate constant data describing the pyrolysis of formic and acetic acids are needed to build reliable kinetic mechanisms for large oxygenated fuels.

There are two main pathways for the decomposition of formic acid [6]; dehydration (R1), and decarboxylation (R2):

$$HCOOH \rightarrow CO + H_2O \qquad (R1)$$
$$HCOOH \rightarrow CO_2 + H_2 \qquad (R2)$$

A number of experimental [6–11] and theoretical [12–15] studies have been carried out on the decomposition of formic acid, including three shock tube studies. Hsu et al. [6] studied the decomposition of formic acid using infrared (IR) laser absorption of CO. They determined the rate constants of both reactions R1 and R2 using a non-linear least square fitting of the measured CO profiles. They found that the branching ratio, k_1/k_2, was ~10 at low temperatures and approaches 1 at 2000 K. Saito et al. [7] studied the thermal decomposition of formic acid in a shock tube using formic acid emission near 3.4 μm, CO emission near 4.6 μm and CO_2 emission near 4.23 μm. Their measurements found that the branching ratio, k_1/k_2, was of order 100 over the entire temperature range (1300–2000 K). The

observed rate constant behaviour agreed with their calculations using the Rice–Ramsperger–Kassel–Marcus (RRKM) weak collision theory. In 2005, Saito et al. [8] reinvestigated the decomposition of the formic acid by monitoring the IR emission of formic acid monomer (5.66 μm), CO (4.63 μm) and CO_2 (4.23 μm). They noted that 10–20% of gaseous formic acid is converted to formic acid dimer, $(HCOOH)_2$, at room temperature and this concentration cannot be neglected. Rate constant results obtained from this study were in reasonable agreement with their previous study [7].

Similar to formic acid, there are two main pathways for the decomposition of acetic acid; decarboxylation (R3) and dehydration (R4):

$$CH_3COOH \rightarrow CH_4 + CO_2 \qquad (R3)$$
$$CH_3COOH \rightarrow CH_2CO + H_2O \qquad (R4)$$
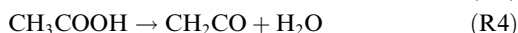
Blake and Jackson [16,17] studied the acetic acid pyrolysis using static and flow systems at temperatures of 733–1053 K and pressures near 1 atm. They concluded that the decarboxylation reaction is first order while the dehydration reaction is second order below 873 K and it exhibits first order behaviour for higher temperatures. Mackie and Doolan [18] studied the thermal decomposition of acetic acid in a single-pulse shock tube. Using gas chromatograph and IR cell analysis of the product gases, they found that the acetic acid decomposed through the two competing pathways, R3 and R4, at approximately equal rates and both rates were first order. Saito et al. [3] used a shock tube to study the thermal decomposition of ethyl acetate which produces acetic acid and ethylene. The branching ratio, k_4/k_3, was measured by comparing the monitored IR emissions from CO_2 (4.23 μm) and H_2O (2.68 μm) and was found to be approximately unity. Another study by Butkovskaya et al. [19] used a flow reactor and IR emission of CO_2 and H_2O to study acetic acid decomposition. They concluded that the k_4/k_3 ratio was two and in agreement with the *ab initio* calculations of Nguyen et al. [20] and Duan and Page [21].

In this work, sensitive and time-resolved laser-absorption measurements of CO, CO_2 and H_2O were used to study the thermal decomposition of formic and acetic acids behind reflected shock waves. The measured time-history profiles were then used to calculate the rate constants of dehydration and decarboxylation reactions for both acids and these rates are compared to available experimental and theoretical data.

2. Experimental details

2.1. Shock tube facility

The experiments were carried out in a high-purity stainless steel shock tube facility at King Abdullah University of Science and Technology (KAUST). The shock tube has an inner diameter of 14.2 cm; the driven section is 9 m long while the driver section length can be varied to a maximum of 9 m. The inner surface of the shock tube is honed and electro-polished to reduce boundary layers and trapped impurities. The incident shock velocity is determined ($\pm 0.1\%$) using five PCB (Model 113B26) piezo-electric pressure transducers (PZT) spaced over the last 1.3 m of the driven section. The shock velocity at the endwall is determined by extrapolating the measured velocity. Typical incident shock attenuation rates ranged from 0.2% to 2%/m for the current experiments. The pre-shock mixture pressure, P_1, is measured using a high-accuracy Baratron pressure transducer, while the pre-shock initial mixture temperature, T_1, is measured using a K-type thermocouple. Reflected shock conditions, P_5 and T_5, are calculated using standard normal-shock relations and thermochemical data taken from the Sandia thermodynamic database [22].

2.2. Mixture preparation

Gas mixtures were prepared manometrically using high-purity argon (99.999%) and Sigma Aldrich's formic ($\geqslant 98\%$) or acetic ($\geqslant 99.7\%$) acids. A freeze–pump–thaw process was used to purify the acids. The acid was first evaporated and introduced into a mixing vessel; argon gas was then slowly flown into the vessel. A magnetically-driven stirrer assembly was used for at least 1 h ensure homogenous mixing. The shock tube was pumped for about 30 min between two successive experiments by a turbo-molecular pump (Varian TV 551), and achieved an ultimate pressure of 2×10^{-5} mbar with out-gassing leak rate of 5×10^{-6} mbar/min.

Since formic and acetic acids tend to adsorb to the surface of shock tube and mixing vessel, Fourier-Transform-Infrared (FTIR) spectroscopy was used to measure the mole fraction of formic/acetic acid in the shock tube prior to the shock-heating process. A multi-pass optical cell, having an effective path-length of 190 cm, was connected to the shock tube driven section through a valve and Teflon pipe. The pre-shock mixture was analyzed with an FTIR spectrometer (VETEX-80V) at a spectral resolution of 0.6 cm^{-1}. The sample compartment of the spectrometer was purged with N_2 to reduce interference absorption from ambient CO_2 and water vapor. The FTIR setup used here has been described previously [23].

Both formic and acetic acids exhibit strong absorption bands near 1105 (v_6) and 1182 cm^{-1} (v_8), as shown in Fig. S1 (Supplementary Material). Formic and acetic acid dimers also have strong absorption features near 1218 and 1295 cm^{-1}, respectively (Fig. S1). Pure formic and acetic acid vapours can contain substantial ($\sim$30–50%) concentration of dimer. The dimer concentration is relatively small in mixtures of acid with argon, as used here. However, it is important to take the dimer concentration into consideration when calculating the initial acid mole fraction. The shock-heating process will convert all dimer to monomer at the reflected shock wave (time zero).

In the current work, the mole fractions of the acid monomers and dimers in the initial mixture were obtained by comparing the FTIR-measured integrated band intensities with values derived from PNNL database [24]. Our measurements indicate that the contribution of the dimer is quite small compared to monomer in the acid/argon mixtures used here; the dimer concentration is less than 10% in all considered cases. The initial concentration of the formic/acetic acid is calculated to be equal to monomer concentration $+ 2 \times$ dimer concentration. The mole fraction values obtained by FTIR spectroscopy are within 50% of the manometric values. Due to adsorption losses, the FTIR measured values are used for rate constant calculations.

2.3. Laser absorption measurements

Three separate optical setups were installed near the shock tube endwall to monitor simultaneously CO, CO_2, and H_2O time-histories. The laser beams from three laser sources were transmitted through optical windows located at a distance 2 cm from the driven section endwall. For all absorption diagnostics, the mole fraction was calculated using the Beer–Lambert law:

$$I/I_0 = \exp(-S\phi X P_5 L), \tag{1}$$

where I is the transmitted laser intensity, I_0 is the incident laser intensity, S (cm^{-2} atm^{-1}) is the line-strength of the transition, ϕ (cm) is the line-shape function, X is the mole fraction of the absorbing species, P_5 (atm) is the total pressure of the gas

behind reflected shock wave and L (cm) is the absorption path length (internal diameter of the shock tube).

Carbon monoxide mole fraction was measured using the R(13) absorption line near 2193.36 cm^{-1} (4.56 μm) in the v_1 fundamental vibrational band of CO. A fixed-wavelength direct absorption strategy was used, where the mid-IR light was generated by a cw quantum cascade laser (QCL) supplied by Alpes Lasers. The argon-broadening parameters for the R(13) transition were taken from [25], whereas line-strength was obtained from the HITRAN database [26].

An external-cavity QCL by Daylight Solutions was used for the laser absorption of carbon dioxide near 2390.52 cm^{-1} (4.18 μm) in the v_3 vibrational band of CO$_2$. High temperature cross-sections of CO$_2$ at the line-centre were measured in our shock tube and verified with previous measurements by Ren et al. [27]. The time resolution of the laser diagnostics used in this study is 0.4 μs.

Water vapour concentration was monitored using a distributed feedback (DFB) diode laser operating near 3416.16 cm^{-1} (2.93 μm) in the v_3 fundamental vibrational band of H$_2$O. The selected transition has relatively high lower-state energy and thus absorption by ambient water vapour is negligible. Absorption cross-sections were measured for the temperature range of interest using our shock tube facility.

3. Results and discussion

Unimolecular decomposition rates were measured for formic and acetic acids using shock tube and laser absorption. For formic acid, the experiments were performed at temperatures of 1234–1821 K, pressures of 1.0 and 6.5 atm and initial concentration of 0.5% in argon. For acetic acid, the pyrolysis experiments were performed at temperatures of 1233–1853 K, pressures of 1.0 and 6.0 atm and initial concentrations of 0.24% and 0.6% in argon.

3.1. Formic acid pyrolysis

Concentration time-histories of CO, CO$_2$ and H$_2$O were measured simultaneously during the pyrolysis of formic acid. Representative traces are shown in Fig. 1. The transmitted intensity is lost at early times due to the large density gradient across the shock wave, leading to a spike in the absorbance near time zero. This is known as the schlieren spike, not shown here. The rate constant, k_1, is calculated using three different approaches. The first and second approach are based on non-linear least square fitting (shown in Fig. 1) of the [CO] and [H$_2$O] profiles, as suggested by Hsu et al. [6].
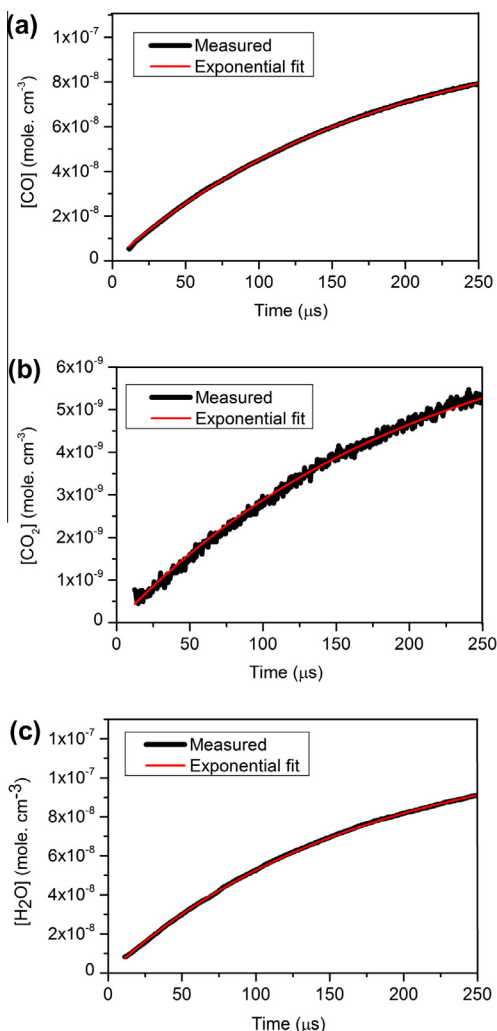

Fig. 1. Measured (a) CO (b) CO$_2$ and (c) H$_2$O concentrations profiles for the decomposition of 0.46% formic acid/Ar at 1532 K and 1.15 atm. Also, shown are the best-fit profiles using the exponential function (Eq. (2)).

$$[CO]_t = a(1 - \exp(-bt)), \qquad (2)$$

where $b = k_1 + k_2$, $a = k_1[FA]_0/b$. The constants a and b are derived from fits to the data. Knowing the initial concentration of formic acid, $[FA]_0$, the first order rate constants, k_1 and k_2, can be calculated. The second order rate constants can be calculated using the total density. An equation, similar to Eq. (2), can also be written for H$_2$O. The rate constants calculated using [CO] and [H$_2$O] profiles are within 8% of each other. The third approach is based on fitting the measured profiles using the Curran et al. [1] dimethyl ether mechanism which includes the pyrolysis reactions of formic acid. The measured CO time-history
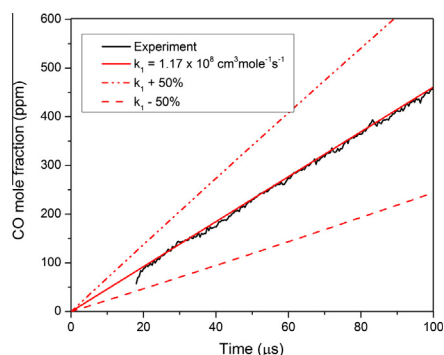
Fig. 2. Measured mole fraction of CO behind reflected shock waves for 0.37% formic acid/Ar pyrolysis at 1396 K and 1.22 atm. Best-fit line using the kinetic mechanism as well as perturbations of ±50% are also presented.

profiles were fit by changing k_1 to achieve a best-fit; Fig. 2 shows an example of fitting the CO profile with the mechanism-simulated profile.

A comparison between the values of k_1 calculated by fitting the [CO] profiles to exponential function (Eq. (2)) and by using the best-fit profiles from the mechanism [1] is shown in Fig. 3. Both methods agree reasonably with each other over the range of temperatures studied here. Similar behaviour was observed for the decarboxylation rate k_2 by comparing the rates obtained by exponential function and mechanism fitting of CO_2 profiles. Sensitivity analyses were performed for CO and CO_2 using Curran et al. [1] mechanism, and are shown in Figs. S2 and S3 (Supplementary Material). The sensitivity is calculated as $S = (\partial X/\partial k_i) \times (k_i/X)$, where X is the local species mole fraction and k_i is the rate constant of the ith reaction. The sensitivity plots show that the dehy-

dration and decarboxylation reactions are dominant at the experimental conditions. However, minor interferences from secondary reactions occur and can become significant at higher temperatures and longer times. Therefore, at temperatures higher than 1500 K, only the initial 50–100 μs of the measured species profiles are used to deduce rate constants. The sensitivity analyses presented in Figs. S2 and S3 show the influence of a 3rd decomposition channel, HCOOH = HCO + OH. This is an energetically inaccessible channel and we think that the rate parameters for this reaction are overestimated in the kinetic mechanism used here and thus shows up being sensitive. This is another reason that we opted to not use the mechanism-fitting method for deducing rate constants. Hsu et al. [6] also concluded that this reaction can be ignored and only R1 and R2 are the main decomposition pathways of formic acid.

Arrhenius plots of the rate constants, calculated based on Eq. (2) fitting, for reactions R1 and R2 are shown in Fig. 4. Excellent signal-to-noise ratio (SNR) was obtained for CO profiles at all cases, however, the SNR of the CO_2 profiles was quite low. This is due to the fact that the branching ratio of formic acid decomposition strongly favours CO formation. The measured rate constants did not exhibit any dependence
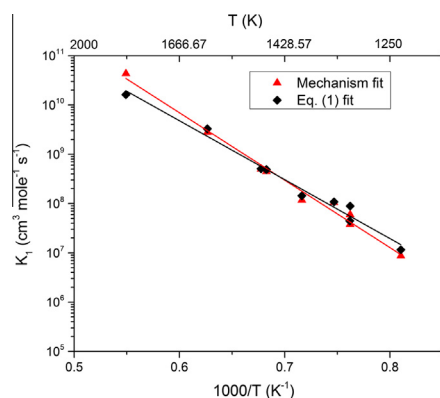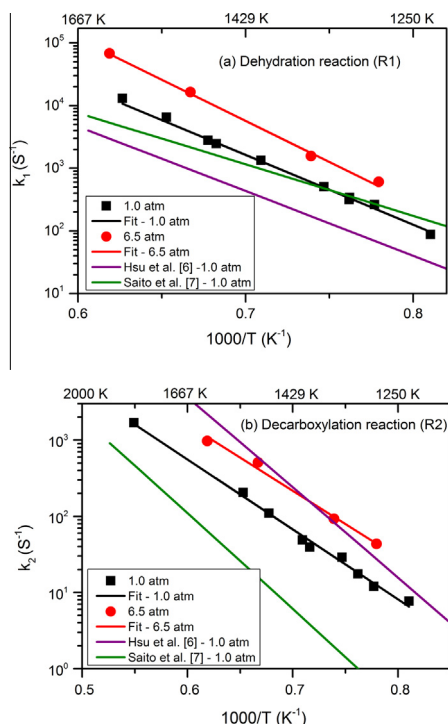

Fig. 3. Comparison of k_1 determined by fitting the CO profiles with an exponential function (Eq. (2)) and by using the best-fit profile from the kinetic mechanism. Solid lines are linear-fit to the data points.

Fig. 4. Comparison of the measured (a) k_1 and (b) k_2 with previous experimental data. Formic acid concentration was 0.5% for both 1 atm and 6.5 atm cases.

on the initial concentration of HCOOH. It can be seen from Fig. 4 that both the dehydration reaction (R1) and the decarboxylation reaction (R2) are in the fall-off range over the measured pressure range (1–6 atm). We have, therefore, plotted the first-order rates of R1 and R2 at different pressures in Fig. 4. Experimental work of Saito et al. [7,8] concluded that k_2 is in the fall-off region whereas k_1 is in the low-pressure limit over 1–5 atm. Their RRKM calculations, on the other hand, predicted that both reactions should be in the falloff region over a pressure range of 1–12 atm. Additional studies at higher pressures are needed to ascertain the fall-off behaviour of the formic acid decomposition reactions. Fitting the experimental data for k_1 and k_2 (black '1.0 atm' and red '6.5 atm' lines in Fig. 4) results in the following first order rate constants:

$$k_1(1\,atm) = 1.03 \times 10^{11} \exp(-25651/T)\,s^{-1}\,(1234–1596\,K)$$
$$k_1(6.5\,atm) = 9.12 \times 10^{12} \exp(-30275/T)\,s^{-1}\,(1283–1616\,K)$$
$$k_2(1\,atm) = 1.79 \times 10^{8} \exp(-21133/T)\,s^{-1}\,(1283–1616\,K)$$
$$k_2(6.5;atm) = 2.73 \times 10^{8} \exp(-20074/T)\,s^{-1}\,(1234–1821\,K)$$

Best-fit lines to the experimental data of Hsu et al. [6] and Saito et al. [7] are also shown in Fig. 4 for comparison with our data. For the rate constant of dehydration reaction (R1), there is good agreement between our 1 atm data and Saito et al. [7] data at temperatures less than 1430 K, while at higher temperatures our measured rate constants are faster by a factor of 2–4. The dehydration rate constant measured by Hsu et al. [6] is lower at all temperatures, though their activation energy is quite similar to our data. The current study exhibits less uncertainty because of the lower reactant concentration, and thus lower influence from secondary reactions, that was possible because of the sensitive laser absorption diagnostics for CO, CO_2 and H_2O. The rate constant for decarboxylation reaction (R2) provided by Saito et al. [7] is lower than that of Hsu et al. [6] by approximately two orders of magnitude. Our measurements fall between these two previous determinations. Comparing Fig. 4(a) and Fig. 4(b), it can be concluded that the $k_1/k_2 \cong 20$ over the entire temperature range studied here.

3.2. Acetic acid pyrolysis

Pyrolysis of acetic acid diluted in argon was studied at temperatures of 1233–1720 K, pressures of 1.0 atm and 6.0 atm and two initial concentrations of acetic acid (0.24% and 0.5%.) As mentioned earlier, acetic acid decomposes via decarboxylation (R3) and dehydration (R4) reactions. The rate constants, k_3 and k_4, of these two reactions were determined by fitting the measured CO_2 and H_2O profiles with simulations from the acetic acid mechanism of Mackie and Doolan

[18]. Figure 5 shows representative time-history profiles of CO_2 and H_2O for the pyrolysis CH_3-COOH. The best-fit profiles give a value of 438 s^{-1} for k_3 and 740 s^{-1} for k_4. This method of determining the rate constant by fitting the measured species profile with the simulated profile was prefered for acetic acid because the pyrolysis mechanism of Mackie and Doolan [18] contains all relevant reactions of acetic acid and its fragments. Sensitivity analyses performed for CO_2 and H_2O (Fig. S4 Supplementary Material) show that the CO_2 profile is only significantly sensitive to the rate constant k_3, while the H_2O profile is primarily sensitive to the rate constant k_4.

Arrhenius plots for both decarboxylation and dehydration reactions of acetic acid pyrolysis are shown in Fig. 6 for a range of pressures and initial concentrations. It can be observed that the first order rate constants of both reactions R3 and R4 show pressure dependence. Thus the decarboxylation and dehydration reactions (R3) and (R4) appear to be in the falloff regime. Fitting the experimental data for k_3 and k_4 (red and black '1.0 atm' and green '6.0 atm' lines in Fig. 6) results in the following first order rate constants:
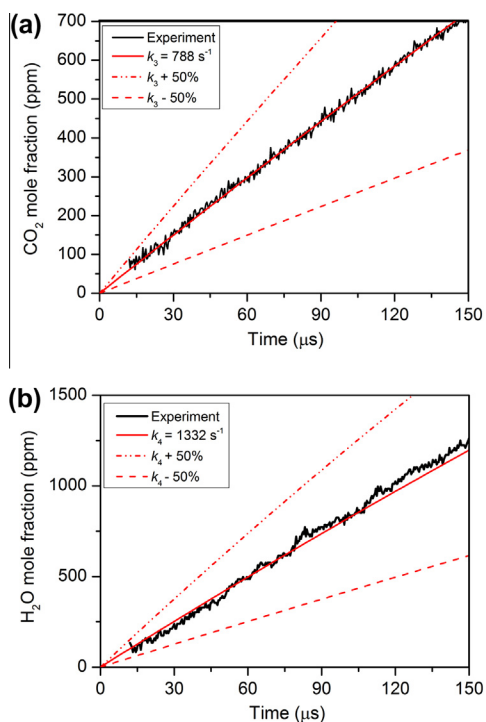

Fig. 5. Measured mole fractions of (a) CO_2 and (b) H_2O for 0.64% acetic acid/Ar pyrolysis at 1435 K and 0.964 atm. Best-fit lines using the kinetic mechanism as well as perturbations of ±50% are also presented.

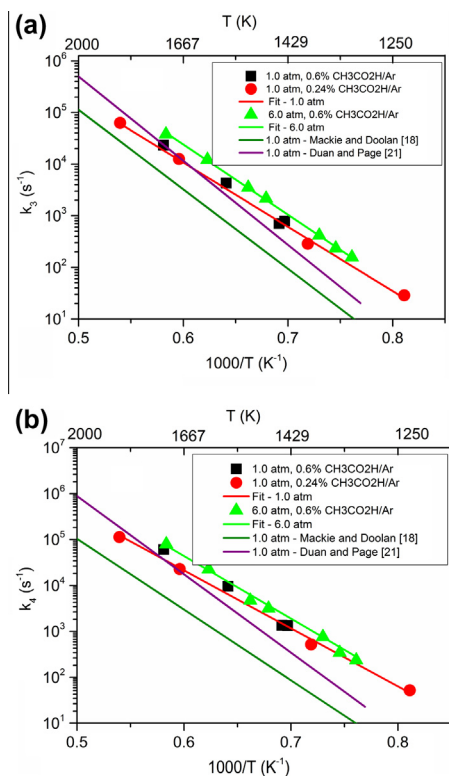Fig. 6. Arrhenius plots of (a) k_3 and (b) k_4 at different conditions (shown in the figure) and comparison with previous studies.

$$k_3(1\,\text{atm}) = 3.18 \times 10^{11} \exp(-28679/T)\,\text{s}^{-1}\,(1233–1851\,\text{K})$$

$$k_3(6\,\text{atm}) = 3.51 \times 10^{12} \exp(-31330/T)\,\text{s}^{-1}\,(1314–1714\,\text{K})$$

$$k_4(1\,\text{atm}) = 7.9 \times 10^{11} \exp(-29056/T)\,\text{s}^{-1}\,(1233–1851\,\text{K})$$

$$k_4(6\,\text{atm}) = 6.34 \times 10^{12} \exp(-31330/T)\,\text{s}^{-1}\,(1314–1714\,\text{K})$$

Our measured rate constant data show that the tendency of the dehydration reaction to occur is about two times higher than that of the decarboxylation reaction, as observed previously by [19–21]. Mackie and Doolan [18], on the other hand, argued that both reactions have about the same probability. It can be also seen from Fig. 6 that there is reasonable agreement, especially at high temperatures, between our measured rate constants (k_3 and k_4) and the theoretical values calculated by Duan and Page [21]. The experimental values measured by Mackie and Doolan [18] are smaller than our results by almost an order of magnitude.

3.3. Uncertainty analysis

Detailed uncertainty analysis is carried out to estimate the overall uncertainty in the measured rate constants. The individual sources of errors in the measured rate constants are: temperatures ($\pm 0.7\%$), the mixture composition ($\pm 50\%$), CO, H_2O and CO_2 absorption coefficients ($\pm 3\%$), wavemeter reading ($\pm 0.005\,\text{cm}^{-1}$), fitting the experimental profiles ($\pm 5\%$), locating time zero ($\pm 0.5\,\mu\text{s}$), the rate constants for secondary reactions $HCOOH \rightarrow HCO + OH$ (uncertainty factor = 4, R1 and R2), $HCOOH + H \rightarrow H_2 + CO + OH$ (uncertainty factor = 4, R1), $HCOOH + H \rightarrow H_2 + CO_2 + H$ (uncertainty factor = 4, R2), $CH_3COOH \rightarrow CH_4 + CO_2$ (uncertainty factor = 4, R4) and $CH_3COOH \rightarrow CH_2CO + H_2O$ (uncertainty factor = 1.86, R4). The effects of these error sources on the rate constant are determined separately. The overall uncertainty is calculated by the root-sum-squared method and found to be $\pm 37\%$ and $\pm 41\%$ for the first-order rate constants of R1 and R2, respectively at 1396 K and 1.22 atm. The uncertainty was calculated to be 32% and 37% for R1 and R2 at 1353 K and 6.8 atm. The estimated overall uncertainties of first-order rate for reactions R3 and R4 are $\pm 29\%$ and $\pm 34\%$, respectively at 1435 K and 0.964 atm. It was also calculated at 1472 K and 6.2 atm and found to be 25% and 31% for R3 and R4, respectively.

4. Conclusions

The rate constants for the decarboxylation and dehydration pathways of formic and acetic acid pyrolysis were measured behind reflected shock waves using CO, CO_2 and H_2O laser absorption. Significantly reduced uncertainties in these rate measurements were achieved because of the high sensitivity and signal-to-noise ratio of the species time-history measurements used in these determinations. The measured rate constants will help provide improved modelling of the decomposition of these two carboxylic acids and will aid in the refinement of detailed kinetic mechanisms of oxygen-containing biofuels.

Appendix A. Supplementary data

Supplementary data associated with this article can be found, in the online version, at http://dx.doi.org/10.1016/j.proci.2014.06.141.

References

[1] H. Curran, S. Fischer, F. Dryer, *Int. J. Chem. Kinet.* 32 (12) (2000) 741–759.
[2] A.T. Blades, *Can. J. Chem.* 32 (4) (1954) 366–372.
[3] K. Saito, T. Sasaki, I. Yoshinobu, et al., *Chem. Phys. Lett.* 170 (4) (1990) 385–388.
[4] V. Vasudevan, *Shock Tube Measurements of Elementary Oxidation and Decomposition Reactions Important in Combustion Using OH, CH and NCN Laser Absorption*, Ph.D. thesis, Stanford University, USA, 2007.
[5] M. Akao, K. Saito, K. Okada, O. Takahashi, K. Tabayashi, *Ber. Bunsenges. Phys. Chem.* 100 (7) (1996) 1237–1241.
[6] D.S.Y. Hsu, W.M. Shaub, M. Blackburn, M.C. Lin, *Proc. Combust. Inst.* 19 (1) (1982) 89–96.
[7] K. Saito, T. Kakumoto, H. Kuroda, S. Torii, A. Imamura, *J. Chem. Phys.* 80 (1984) 4989.
[8] K. Saito, T. Shiose, O. Takahashi, Y. Hidaka, F. Aiba, K. Tabayashi, *J. Phys. Chem. A* 109 (24) (2005) 5352–5357.
[9] P.G. Blake, H.H. Davies, G.E. Jackson, *J. Chem. Soc. B: Phys. Org.* (1971) 1923–1925.
[10] H. Su, Y. He, F. Kong, W. Fang, R. Liu, *J. Chem. Phys.* 113 (2000) 1891.
[11] T. Ebata, A. Fujii, T. Amano, M. Ito, *J. Phys. Chem.* 91 (24) (1987) 6095–6097.
[12] J. Francisco, *J. Chem. Phys.* 96 (1992) 1167.
[13] J.-G. Chang, H.-T. Chen, S. Xu, M. Lin, *J. Phys. Chem. A* 111 (29) (2007) 6789–6797.
[14] I.d.P.R. Moreira, *J. Mol. Struct.: Theochem.* 466 (1-3) (1999) 119–126.
[15] Y. Kurosaki, K. Yokoyama, Y. Teranishi, *Chem. Phys.* 308 (3) (2005) 325–334.
[16] P.G. Blake, G.E. Jackson, *J. Chem. Soc. B: Phys. Org.* (1968) 1153–1155.
[17] P.G. Blake, G.E. Jackson, *J. Chem. Soc. B: Phys. Org.* (1969) 94–96.
[18] J.C. Mackie, K.R. Doolan, *Int. J. Chem. Kinet.* 16 (5) (1984) 525–541.
[19] N. Butkovskaya, G. Manke, D. Setser, *J. Phys. Chem.* 99 (28) (1995) 11115–11121.
[20] M.T. Nguyen, D. Sengupta, G. Raspoet, L.G. Vanquickenborne, *J. Phys. Chem.* 99 (31) (1995) 11883–11888.
[21] X. Duan, M. Page, *J. Am. Chem. Soc.* 117 (18) (1995) 5114–5119.
[22] R. Kee, F. Rupley, J. Miller, The Chemical Thermodynamic Data Base, Report No. SAND87-8215B.UC-4, Sandia National Laboratory, 1987.
[23] E.-t. Es-sebbar, Y. Benilan, A. Farooq, *J. Quant. Spectrosc. Radiat. Transfer* 115 (2013) 1–12.
[24] S.W. Sharpe, T.J. Johnson, R.L. Sams, P.M. Chu, G.C. Rhoderick, P.A. Johnson, *Appl. Spectrosc.* 58 (12) (2004) 1452–1461.
[25] W. Ren, A. Farooq, D. Davidson, R. Hanson, *Appl. Phys. B* 107 (3) (2012) 849–860.
[26] L. Rothman, I. Gordon, Y. Babikov, et al., *J. Quant. Spectrosc. Radiat. Transfer* 130 (2013) 4–50.
[27] W. Ren, R. Spearrin, D. Davidson, R. Hanson, in: *8th U.S. National Combustion Meeting*, University of Utah, USA, May, 2013.